Check for updates

DOI: 10.1111/phor.12438

ORIGINAL ARTICLE

Generation of concise 3D building model from dense meshes by extracting and completing planar primitives

Xinyi Liu[1] | Xianzhang Zhu[1,2,3] | Yongjun Zhang[1] | Senyuan Wang[1] | Chen Jia[1]

[1]Wuhan University, Wuhan, China

[2]Changjiang Spatial Information Technology Engineering Co., Ltd, Wuhan, China

[3]Water Resources Information Perception and Big Data Engineering Research Center of Hubei Province, Wuhan, China

Correspondence
Xianzhang Zhu and Yongjun Zhang, Wuhan University, Wuhan, China.
Email: zxzorigin@whu.edu.cn; zhangyj@whu.edu.cn

Funding information
Basic Research Strengthening Program of China (173 Program), Grant/Award Number: 2020-JCJQ-ZD-015-00-04; National Natural Science Foundation of China, Grant/Award Number: 41871368; Science and Technology Major Project of Hubei Province, Grant/Award Number: 2021AAA010; Zhizhuo Research Fund on Spatial-Temporal Artificial Intelligence, Grant/Award Number: ZZJJ202206

Abstract

The generation of a concise building model has been and continues to be a challenge in photogrammetry and computer graphics. The current methods typically focus on the simplicity and fidelity of the model, but those methods either fail to preserve the structural information or suffer from low computational efficiency. In this paper, we propose a novel method to generate concise building models from dense meshes by extracting and completing the planar primitives of the building. From the perspective of probability, we first extract planar primitives from the input mesh and obtain the adjacency relationships between the primitives. Since primitive loss and structural defects are inevitable in practice, we employ a novel structural completion approach to eliminate linkage errors. Finally, the concise polygonal mesh is reconstructed by connectivity-based primitive assembling. Our method is efficient and robust to various challenging data. Experiments on various building models revealed the efficacy and applicability of our method.

KEYWORDS
concise building model, planar primitive, polygonal mesh, primitive assembling, structural completion

© 2023 Remote Sensing and Photogrammetry Society and John Wiley & Sons Ltd.

INTRODUCTION

The demand for three-dimensional (3D) building modelling of real environments is now ubiquitous in many applications, such as smart cities (Yang & Lee, 2017), virtual reality (Bruno et al., 2010) and navigation (Biljecki et al., 2015). Powered by advanced laser scanning, photogrammetry, computer vision and other technologies, this increasing complexity and data volume of 3D building models creates great pressure on storage, visualisation, transmission and subsequent applications. To relieve this pressure, many 3D engineers and researchers have devoted themselves to exploring how to represent buildings more concisely. However, due to the increasing complexity of geometric structures and the various defects corrupted by noise pollution and non-building object occlusion, the automatic generation of concise building models looks to be a long-standing challenge.

The practice of concise building modelling entails not only representing the building concisely but also approximating the original building structure. Mesh simplification and polygonisation are the two most fundamental techniques available to address this task. Mesh simplification (Garland & Heckbert, 1997; Li & Nan, 2021; Lindstrom, 2000; Salinas et al., 2015) takes dense meshes generated by combining point clouds and surface reconstruction algorithms as inputs and deletes the redundant vertices and faces while preserving the structures. Polygonisation (Bauchet & Lafarge, 2020; Boulch et al., 2014; Bouzas et al., 2020; Nan & Wonka, 2017) generally segments planes from point clouds or dense meshes and assembles them to approximate the original structures. Both mesh simplification and polygonisation can generate lightweight meshes effectively. However, the currently available methods commonly have the following problems:

1. Redundant representation. The primitives are not represented in the simplest form but rather contain redundant vertices and faces.
2. Incomplete structures. Some structures are missing and accompanied by incorrect adjacencies due to undetectable primitives, low precision boundary information and complex structures.
3. Unstructured. The output meshes do not contain any adjacency relationships and attribute information of the primitives.
4. Weak robustness. The computation and memory are too intensive for dealing with highly complex buildings.

To address the above problems, we present a novel method that aims to generate concise building models from dense building meshes automatically. The input dense building mesh can be generated by surface reconstruction of LiDAR point clouds or photogrammetric point clouds and can be watertight or with borders. Our proposed method first extracts planar primitives with adjacency relationships through primitive determination. Then, the linkage errors caused by missing primitives are addressed by an iterative structural completion approach. Finally, the concise polygonal mesh is reconstructed by connectivity-based primitive assembling. The main contributions of our proposed method are as follows:

1. The proposed method casts planar face subset extraction as a geometric rigidity measuring problem, which makes it capable of extracting accurate planar primitives without requiring a pre-setting threshold.
2. A two-stage gradual region growing algorithm is proposed to obtain accurate adjacency relationships between the primitives. The primitive is grown to the neighbourhood by a gradually increased angle threshold, so as to reduce the influence of the unsmooth surface.
3. The proposed method employs a novel structural completion approach to address the problem of primitive loss and structural defects. Those adjacent primitive pairs detected as structural defects will be deducted and completed iteratively, which makes the final primitive assembling not constrained by linkage errors. Therefore, the proposed method is efficient and robust to various challenging data.

14779730, 2023, 181, Downloaded from https://onlinelibrary.wiley.com/doi/10.1111/phor.12438 by Wuhan University, Wiley Online Library on [08/03/2024]. See the Terms and Conditions (https://onlinelibrary.wiley.com/terms-and-conditions) on Wiley Online Library for rules of use; OA articles are governed by the applicable Creative Commons License

The remainder of this paper is organised as follows. The "Related Works" section briefly reviews the related published works. The "Methodology" section introduces in detail the methodology of our proposed generation method for concise building models. The "Experiments and Analysis" section presents and discusses the experimental results and compares the performance of our method to that of existing methods. The "Application to Urban Building Modelling" section presents an example application of our method for urban building modelling. Finally, the "Conclusions" section concludes this paper.

RELATED WORKS

Over the past few decades, numerous studies have addressed various aspects of reconstructing building models. A great deal of work continues today associated with many 3D processing techniques. Particularly crucial is finding ways to simplify the representation of building models in the current era of data explosion. This section reviews the related literature that focuses on the key technologies addressed in this paper, including plane segmentation, planar primitive-based building reconstruction, mesh segmentation and mesh simplification.

Plane segmentation

Plane segmentation is to extract the point set constituting the planar structure from the disordered point cloud. Planes constitute most of the structures in 3D space, especially man-made objects, which makes plane segmentation a basic technique in 3D processing. In general, the plane segmentation techniques can be categorised into three groups, feature clustering, region growing and model fitting. Feature-clustering-based approaches group the adjacent points of certain similar geometric properties (Biosca & Lerma, 2008; Sampath & Shan, 2006). Region-growing-based methods usually select one or more seed points and grow them based on some predefined similar criteria (normal vector, curvature, etc.) (Besl & Jain, 1988; Nurunnabi et al., 2012; Rabbani et al., 2006). For the model-fitting-based approaches, planar parameters are approximated from the point cloud utilising voting techniques (Awwad et al., 2010; Schnabel et al., 2007; Sevgen & Karsli, 2020; Tarsha-Kurdi et al., 2007).

Scanline analysis and energy optimisation, which are proved to be effective in 2D image processing, can also be applied to 3D plane segmentation. Scanline analysis groups scan profiles that are derived by segmenting point clouds through a merging operation according to some similarity feature (Nguyen et al., 2019). As to the energy optimisation, initial planes are generated via geometric-based techniques and then, points' labels are optimised by establishing an energy function (Pham et al., 2014; Yan et al., 2014). In recent years, the voxel has become a new trend in 3D processing for its high computational efficiency. Vo et al. (2015) used voxels as the only basic units and grouped them with similar saliency features. Dong et al. (2018) proposed an approach that forms basic units from combined multi-scale planar supervoxels and individual points and optimises the initial planes through global energy optimisation. However, when the noise level is severe and the scene is large, precise plane fitting remains a challenge to be addressed.

Planar primitive-based building reconstruction

Extracting geometric primitives is commonly used in building reconstruction (Song et al., 2021). Planar primitive-based building reconstruction assumes that buildings are formed by planes and can be reconstructed by a regular arrangement of planes (Li et al., 2020; Monszpart et al., 2015). In order to obtain the vertices, edges and faces of the building model, researchers analyse the adjacency graph between planar primitives and then fit polygons by connecting the boundary points (Chen & Chen, 2008; Schindler et al., 2011). However,

14779730, 2023, 181, Downloaded from https://onlinelibrary.wiley.com/doi/10.1111/phor.12438 by Wuhan University, Wiley Online Library on [08/03/2024]. See the Terms and Conditions (https://onlinelibrary.wiley.com/terms-and-conditions) on Wiley Online Library for rules of use; OA articles are governed by the applicable Creative Commons License

adjacency graphs often are not completely correct. Arikan et al. (2013) proposed a semiautomatic reconstruction method, which completes the missing structure through manual interaction. Considering that plane segmentation directly affects the regularisation of the planar parameters, several methods introduced plane regularisation to improve the integrity of planar primitives (Oesau et al., 2016). Wang et al. (2020) adopted a surface optimisation scheme that takes into account structural closure constraints and the adjacency of candidate planes, with the final 3D polygonal surfaces of the building enforced to be consistent with a priori geometric structures.

Another common way to generate polygonal building meshes is known as plane slicing. These methods use detected planar primitives to slice the 3D space into a convex polyhedral cell complex, and the output surface mesh is reconstructed by selecting the polygonal faces of the cells that are part of the surface (Boulch et al., 2014; Chauve et al., 2010). PolyFit (Nan & Wonka, 2017) casts the reconstruction as a binary labelling problem. The optimal candidate faces are selected from planar primitives, which then are combined to generate manifold polygonal surface models. Bauchet and Lafarge (2020) designed a kinetic data structure to partition 3D space into convex polyhedrons, where convex planar polygons are grown at constant speed until they collide and create polyhedrons. In addition, Bouzas et al. (2020) presented a novel polygonisation approach whereby the planar primitives are detected through mesh segmentation. Polygonisation is then employed based on approximation of the original mesh with a candidate set of planar polygonal faces. However, these methods are highly dependent on the detected planar primitives, and spurious artefacts are easily created due to the constraint of the manifold.

Mesh simplification

Mesh simplification aims to generate concise meshes by simplifying dense meshes reconstructed from points. Based on the differences in their strategies, the existing mesh simplification methods mainly can be divided into two categories: decimation and approximation.

The decimation methods simplify dense meshes by removing a large number of homogeneous faces. Edge collapse is the most commonly used technique, which deletes vertices (determined by using some local geometric error metrics) until it reaches a target number of faces (Cohen et al., 2003; Garland & Heckbert, 1997; Lindstrom, 2000; Zelinka & Garland, 2002). Salinas et al. (2015) detected a set of planar proxies from dense meshes as constraints to better preserve the piecewise-planar structure of objects. Li and Nan (2021) proposed a refined mesh decimation method based on mesh filtering preprocessing and a hierarchical error metric by which the detected planes could be well preserved in the edge collapse iterations.

The approximation methods use mesh optimisation and remeshing to approximate the original dense mesh. For example, Cohen-Steiner et al. (2004) reconstructed a new mesh that connected the detected planes using the adjacency inferred from the original mesh. Marinov and Kobbelt (2005) proposed an integral error metric that was designed to derive a subdivision control mesh whose structures are aligned to some detected geometric elements.

These methods are efficient and reliable to some extent, but their simplified results always contain drastic topological alterations. Furthermore, the primitives cannot be formed easily and the simplified mesh is not structured because no adjacency relationships exist between the primitives.

METHODOLOGY

The framework for our method is designed as a three-stage process: (1) primitive determination, (2) structural deduction and (3) polygonal mesh reconstruction. Figure 1 illustrates its workflow.

14779730, 2023, 181, Downloaded from https://onlinelibrary.wiley.com/doi/10.1111/phor.12438 by Wuhan University, Wiley Online Library on [08/03/2024]. See the Terms and Conditions (https://onlinelibrary.wiley.com/terms-and-conditions) on Wiley Online Library for rules of use; OA articles are governed by the applicable Creative Commons License

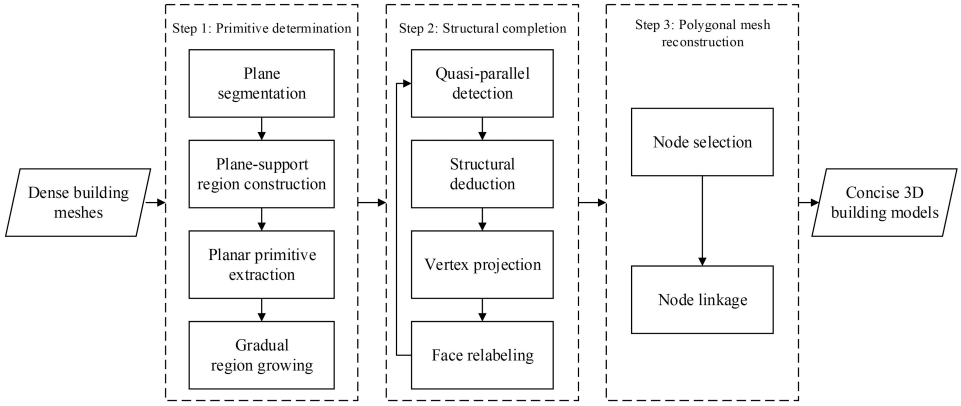

FIGURE 1 The workflow of the proposed method.

Primitive determination

The proposed primitive determination approach aims to extract structural primitives with physically meaningful labels and obtain the adjacency relationships between the primitives. A building, as a man-made object, is mainly composed of planar components in most urban scenes. Instead of searching for partition mesh faces directly based on region growing or clustering algorithms, we find plane-support regions first based on the plane segmentation results of the mesh vertices. Then, an a contrario model is established to validate each planar mesh face subset from the plane-support regions. Finally, a gradual region growing operation is employed to label all the mesh faces into planar primitives so that the adjacency relationships between the primitives can be obtained.

Plane-support regions

The segmentation method based on mesh faces is easily affected by occlusion and normal mutation, resulting in incomplete planar structures. In contrast to that, plane segmentation for 3D points is less constrained by the adjacency relationship so is able to detect complete planar structures better. A novel plane segmentation method (QTPS), which was introduced in our previous paper and proved to be efficient and robust (Zhu et al., 2021), is employed in this part to partition mesh vertices into planes. For each segmented vertex subset, we collect the 1-ring neighbour faces of each inlier vertex to construct the plane-support region. Figure 2 illustrates an example of the detected planes and their corresponding plane-support regions. Each of the faces can be collected into different plane-support regions.

Primitive extraction

Under the background of a contrario, the gestalt, which is defined as the occurrence of any basic structure or grouping law, is independent of each other in the condition of null hypothesis. When the Helmholtz principle is violated as the expected value of the number of false alarms (NFA) is less than 1, a gestalt thus occurs. The a contrario can be adopted to model the structures as gestalts according to the Helmholtz principle and ε-meaningful events. Specifically, from the probabilistic perspective, the Helmholtz principle explains why some gestalts can immediately attract human attention visually (Desolneux et al., 2007). A contrario models have been mostly designed for detecting low-level structures. Typical examples include 2D line segments (von Gioi et al., 2010),

14779730, 2023, 181, Downloaded from https://onlinelibrary.wiley.com/doi/10.1111/phor.12438 by Wuhan University, Wiley Online Library on [08/03/2024]. See the Terms and Conditions (https://onlinelibrary.wiley.com/terms-and-conditions) on Wiley Online Library for rules of use; OA articles are governed by the applicable Creative Commons License

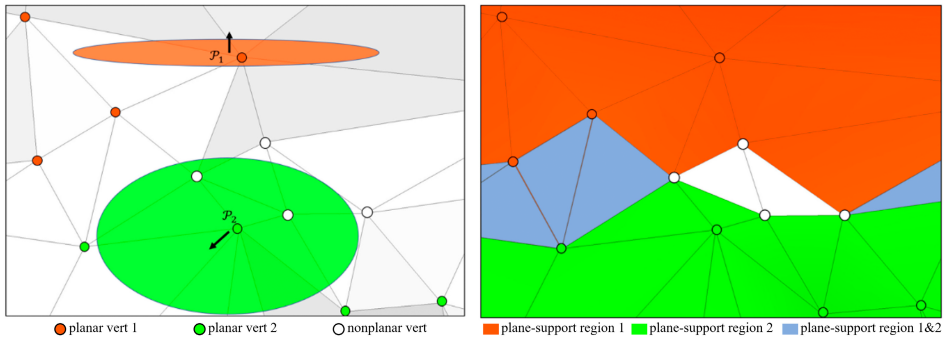

FIGURE 2 Detected planes and their corresponding plane-support regions. Vertices within the same planes are shown in the same colour while non-planar vertices are shown in white. A face is collected into the corresponding plane-support region of the plane if a vertex contained in the face is partitioned into the plane.

vanishing points (Almansa et al., 2003), rigid sets of point matches (Wan et al., 2019) and planar patches (Bughin & Almansa, 2010), etc. Our method contains an a contrario model for detecting planar primitives with precise plane-fitting parameters from the plane-support regions.

In our proposed method, the planar primitives are composed of faces and only the plane-support regions are used for planar primitive detection. Inspired by Desolneux et al. (2007), planar primitives are detected as outliers of the background model, which is reduced to the simplest of all, so-called white noise. More formally, a null hypothesis H_0 is defined, which means that the normal of all the faces in the plane-support region $\mathcal{R}$ is assumed to be independent. Hence, the normal angles between a face $\mathcal{F}$ and a planar model $\mathcal{P}$ ($ax + by + cz + d = 0$) satisfy $0 \le Angle(\mathcal{F}, \mathcal{P}) \le \pi / 2$.

An atom event $e_i(\sigma)$ is defined as the occurrence of the ith face $\mathcal{F}_i$ of which $Angle(\mathcal{F}_i, \mathcal{P})$ is less than θ. Under null hypothesis H_0, the probability of $e_i(\theta)$ can be calculated as:

$$\text{Prob}\left(Angle(\mathcal{F}_i, \mathcal{P}) \le \sigma \,|\, H_0\right) = 2\sigma / \pi. \tag{1}$$

For a plane-support region $\mathcal{R}$, there are many arbitrary face subsets to be formed as potential planar primitives. The $\mathcal{P}$-rigidity of a face subset $\mathcal{r} \subseteq \mathcal{R}$ and $\mathcal{F}_i \in \mathcal{r}$ are defined as:

$$\begin{cases} \alpha_{\mathcal{P}}(\mathcal{r}) = \max\limits_{\mathcal{F}_i \in \mathcal{r}} \alpha_{\mathcal{P}}(\mathcal{F}_i) \\ \alpha_{\mathcal{P}}(\mathcal{F}_i) = 2Angle(\mathcal{F}_i, \mathcal{P})/\pi \end{cases} \tag{2}$$

where $\alpha_{\mathcal{P}}(\mathcal{r})$ gives a probabilistic rigidity measurement to $\mathcal{r}$. The global $\mathcal{P}$-rigidity of $\mathcal{R}$ can be calculated by minimising $\alpha_{\mathcal{P}}(\mathcal{r})$. To find such a planar model $\mathcal{P}$ more efficiently, $\mathcal{P}$ is determined by one of the faces in $\mathcal{R}$.

The planar geometric consistency evaluation of a face subset $\mathcal{r}$ is designed from the perspective of probability. Specifically, $\mathcal{r}$ is defined as α-rigid for a planar model $\mathcal{P}$ if $\alpha_{\mathcal{P}}(\mathcal{r}) \le \alpha$. The face that determines $\mathcal{P}$ satisfies $\alpha_{\mathcal{P}}(\mathcal{F}_i) = 0$ and $\text{Prob}\left(\alpha_{\mathcal{P}}(\mathcal{F}_i) \le \alpha \,|\, H_0\right) = 1$. Combining equations (1) and (2), the conditional probability $\text{Prob}\left(\alpha_{\mathcal{P}}(\mathcal{r}) \le \alpha \,|\, H_0\right)$ can be calculated as follows:

$$\begin{aligned} \text{Prob}\left(\alpha_{\mathcal{P}}(\mathcal{r}) \le \alpha \,|\, H_0\right) &= \prod_{\mathcal{F}_i \in \mathcal{r}} \text{Prob}\left(\alpha_{\mathcal{P}}(\mathcal{F}_i) \le \alpha \,|\, H_0\right) \\ &= \prod_{\mathcal{F}_i \in \mathcal{r}} \text{Prob}\left(Angle(\mathcal{F}_i, \mathcal{P}) \le \alpha \cdot \pi \,|\, H_0\right) = \alpha^{k-1} \end{aligned} \tag{3}$$

14779730, 2023, 181, Downloaded from https://onlinelibrary.wiley.com/doi/10.1111/phor.12438 by Wuhan University, Wiley Online Library on [08/03/2024]. See the Terms and Conditions (https://onlinelibrary.wiley.com/terms-and-conditions) on Wiley Online Library for rules of use; OA articles are governed by the applicable Creative Commons License

where k is the number of faces in $\mathscr{F}$ and k satisfies $k \geq 2$.

The next step is to measure the meaningfulness of $\mathscr{F}$ by computing its NFA. Under the null hypothesis H_0, the NFA of an α-rigid face subset $\mathscr{F} \subseteq \mathcal{R}$ is defined as:

$$\mathrm{NFA}\left(\alpha_{\mathcal{P}}(\mathscr{F}) \leq \alpha \mid H_0\right) = N_{tests} \cdot \mathrm{Prob}\left(\alpha_{\mathcal{P}}(\mathscr{F}) \leq \alpha \mid H_0\right) \tag{4}$$

where N_{tests} is the number of potential tests in $\mathcal{R}$. According to a contrario, H_0 is rejected while $\mathscr{F}$ is accepted as an ε-meaningful face subset if and only if $\mathrm{NFA}\left(\alpha_{\mathcal{P}}(\mathscr{F}) \leq \alpha \mid H_0\right) \leq \varepsilon$.

Considering that each of the faces in $\mathcal{R}$ can be selected to determine a planar model and $\mathscr{F}$ contains at least two faces, N_{tests} satisfies the following inequality:

$$N_{tests} \leq (n-1) \cdot \binom{n}{k} \cdot \binom{k}{1} \tag{5}$$

where $(n-1)$ is the number of choices for k, $\binom{n}{k}$ is the number of possible $\mathscr{F}$ with size k from size n of $\mathcal{R}$ and $\binom{k}{1}$ is the number of possible planar models in $\mathscr{F}$. N_{tests} can be estimated from the right-hand side of the inequality that enables it to adapt to various mesh sizes. Combining equations (4) and (5), we have:

$$\mathrm{NFA}\left(\alpha_{\mathcal{P}}(\mathscr{F}) \leq \alpha \mid H_0\right) \leq (n-1) \cdot \binom{n}{k} \cdot \binom{k}{1} \cdot \alpha^{k-1}. \tag{6}$$

According to Desolneux et al. (2007), the planar primitive in $\mathscr{F}$ is detectable by human sight if $\mathscr{F}$ is 1-meaningful, $\mathrm{NFA}\left(\alpha_{\mathcal{P}}(\mathscr{F}) \leq \alpha \mid H_0\right) \leq 1$.

For each plane-support region, the optimal face subset $\overline{\mathscr{F}}$ and its corresponding optimal planar model $\overline{\mathcal{P}}$ are obtained by minimising NFA. $\overline{\mathscr{F}}$ is added to the planar primitive candidate set, denoted as $\Upsilon = \left\{\overline{\mathscr{F}}_1, \ldots, \overline{\mathscr{F}}_n\right\}$, if its NFA value is less than or equal to 1. Once a face is partitioned into Υ, it is removed from other plane-support regions that contain it.

Then we further screen the planar primitives in Υ according to their area and topological importance. For a $\overline{\mathscr{F}} \subseteq \Upsilon$, instead of calculating the sum of all inlier face areas, we partition those faces in $\overline{\mathscr{F}}$ into blocks ($\overline{\mathscr{F}} = \left\{\mathcal{B}_1, \ldots, \mathcal{B}_n\right\}$), where each block contains a continuous set of faces, and calculate the normalised implicit area of $\overline{\mathscr{F}}$ by the following equation:

$$\varphi(\overline{\mathscr{F}}) = \arctan\left(Area\left(\underset{\mathcal{B}_i \in \overline{\mathscr{F}}}{\mathrm{argmax}}\left(Area\left(\mathcal{B}_i\right)\right)\right)\right) \bullet 2/\pi \tag{7}$$

where $Area\left(\mathcal{B}_i\right)$ is the sum of the face areas in $\mathcal{B}_i$. This step is necessary because discrete faces may not belong to the same primitive.

Furthermore, the topological importance of $\overline{\mathscr{F}}$ is calculated based on its neighbouring primitives, which are collected by the 3-ring neighbourhood of the inlier faces and denoted as $\mathcal{R}^c(\overline{\mathscr{F}}) = \left\{\overline{\mathscr{F}}_1^c, \ldots, \overline{\mathscr{F}}_n^c\right\}$. We consider the topological importance of $\overline{\mathscr{F}}$ is positively correlated with the average angle between $\mathscr{F}$ and $\mathcal{R}^c(\overline{\mathscr{F}})$. Thus, the normalised topological importance of $\overline{\mathscr{F}}$ is calculated as follows:

$$\psi(\overline{\mathscr{F}}) = \begin{cases} \dfrac{\sum_{\overline{\mathscr{F}}_i^c \in \mathcal{R}^c(\overline{\mathscr{F}})} Angle\left(\overline{\mathcal{P}}, \overline{\mathcal{P}}^c\right)}{\left|\mathcal{R}^c(\overline{\mathscr{F}})\right|} \cdot \dfrac{2}{\pi}, \text{if } \left|\mathcal{R}^c(\overline{\mathscr{F}})\right| > 1 \\ 0, \text{if } \left|\mathcal{R}^c(\overline{\mathscr{F}})\right| \leq 1 \end{cases} \tag{8}$$

14779730, 2023, 181, Downloaded from https://onlinelibrary.wiley.com/doi/10.1111/phor.12438 by Wuhan University, Wiley Online Library on [08/03/2024]. See the Terms and Conditions (https://onlinelibrary.wiley.com/terms-and-conditions) on Wiley Online Library for rules of use; OA articles are governed by the applicable Creative Commons License

where $\overline{\mathcal{P}}$ and $\overline{\mathcal{P}}_i^c$ are the corresponding planar models of $\overline{r}$ and $\overline{r}_i^c$, respectively, $|\mathcal{R}^c(\overline{r})|$ is the size of $\mathcal{R}^c(\overline{r})$.

Here $\overline{r}$ is extracted as a valid planar primitive if it satisfies the following condition:

$$\varphi(\overline{r}) + \psi(\overline{r}) \geq \lambda \tag{9}$$

where λ is the threshold of the conditional equation. The tolerance to small area primitives increases when the topological importance is large and vice versa. λ can be set according to the minimum area required for the primitives without adjacency. In this way, we not only can screen out unnecessary primitives with a small area but also preserve detailed connective structures.

Gradual region growing

To determine the adjacency relationships between the planar primitives accurately, we designed a two-stage gradual region growing strategy to partition the remaining faces that are not being labelled into the existing planar primitives.

In our growing approach, an unlabelled face $\mathcal{F}_c$ that is neighboured to the seed face $\mathcal{F}_s$ should be partitioned into $\overline{r}_s$, which is the associated planar primitive of $\mathcal{F}_s$, if it satisfies one of the following two conditions:

$$\begin{cases} Angle(\mathcal{F}_c, \mathcal{F}_s) \leq \theta \\ Angle(\mathcal{F}_c, \overline{\mathcal{P}}_s) \leq \theta \end{cases} \tag{10}$$

where $\overline{\mathcal{P}}_s$ is the corresponding planar model of $\overline{r}_s$, θ is the threshold of the angle for a valid growth. Gradual region growing uses an iterative process to gradually increase θ from θ_{sta} to $\pi / 2$. θ is increased to $\theta \cdot \mu$ ($\mu > 1$) in each iteration and the iterative process ends when all the faces have been partitioned into the planar primitives.

Figure 3 illustrates the procedure of the gradual region growing. For each extracted planar primitive, all the inlier faces are selected as seeds to find the neighbouring unlabelled faces. For the first stage, the 3-ring neighbourhood is used to find the neighbouring unlabelled faces of a seed face, which not only improves the efficiency of the growing process but also better preserves the real boundary of the planar primitive. The growing results of increasing θ by iteration are shown in Figure 4. However, some of the faces that belong to the same planar primitive may not be continuous, which leads to ambiguity between the planar primitives. Hence, in the second stage, for each planar primitive, all faces except for the continuous face subset of the maximum area within the planar primitive are reset to the unlabelled state, and then new planar primitives are extracted from these unlabelled faces. Finally, the 1-ring neighbourhood is used to support the gradual region growing process. Different from the traditional mesh segmentation method, the proposed approach focuses more on obtaining the adjacency relationships between the primitives through the primitive labels of adjacent faces. Hence, our method labels all faces even if they are on some non-planar structures. The advantage of this strategy is that it does not need to grow and collide planes, which greatly improves the efficiency of plane assembling.

Structural completion

Although the proposed primitive determination approach can provide precise primitives with adjacency relationships, some building primitives are difficult to detect for various reasons (noise effect, non-planar, small structure, etc.).

14779730, 2023, 181, Downloaded from https://onlinelibrary.wiley.com/doi/10.1111/phor.12438 by Wuhan University, Wiley Online Library on [08/03/2024]. See the Terms and Conditions (https://onlinelibrary.wiley.com/terms-and-conditions) on Wiley Online Library for rules of use; OA articles are governed by the applicable Creative Commons License

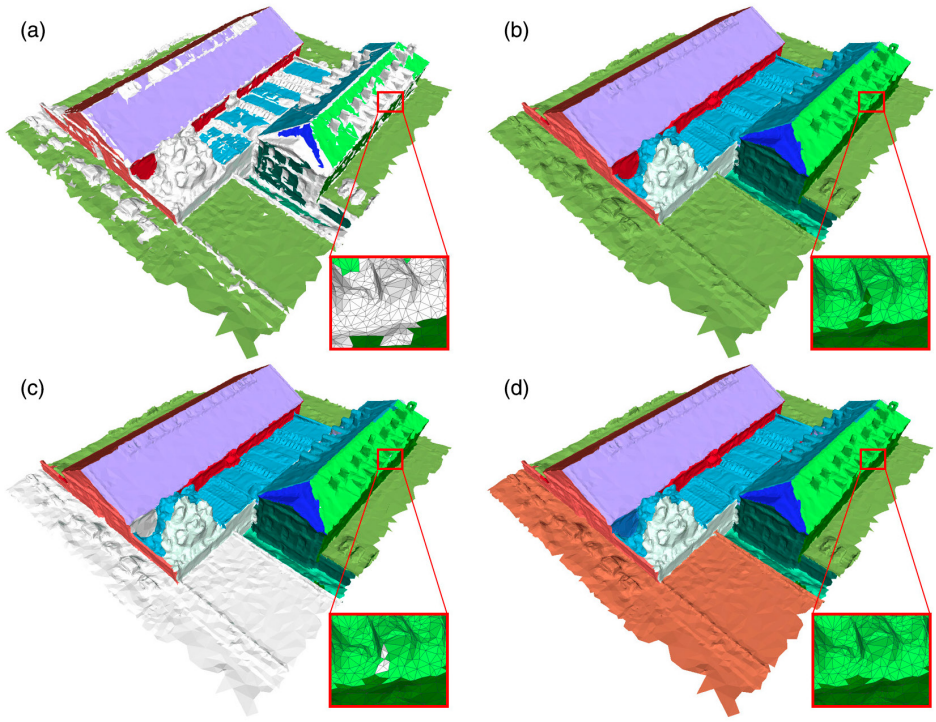

FIGURE 3 Illustration of gradual region growing process: (a) initial planar primitives; (b) gradual region growing based on the 3-ring neighbourhood; (c) reset discontinuous faces to unlabelled state; and (d) the final results.

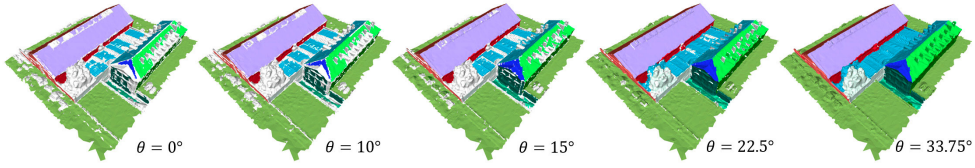

FIGURE 4 Gradual region growing based on the 3-ring neighbourhood, where $\mu = 1.5$ and $\theta_{sta} = 10°$.

The missing primitives not only make the model structure incompletely recoverable but also lead to incorrect adjacency. A serious case in this paper is that two nearly parallel planar primitives were adjacent. To handle this problem, we used a structural completion approach that deducts new planar primitives for each of the incorrect adjacent primitive pairs. The final completed model structure then is recovered through an iterative process.

Vertex definition

Each of the segmented planar primitives contains a set of continuous faces. In accordance with Lafarge and Alliez (2013), we divided the vertices into three structural types, planar, crease and corner, as shown in Figure 5.

Denote $\mathcal{S}_i = \{\overline{r}_1, \ldots, \overline{r}_n\}$ as the associated primitive set of the ith vertex $\mathcal{V}_i$, and $\mathcal{S}_i$ is obtained by collecting the associated primitives of $\mathcal{V}_i$'s 1-ring neighbouring faces. The structural type of $\mathcal{V}_i$ is defined as:

14779730, 2023, 181, Downloaded from https://onlinelibrary.wiley.com/doi/10.1111/phor.12438 by Wuhan University, Wiley Online Library on [08/03/2024]. See the Terms and Conditions (https://onlinelibrary.wiley.com/terms-and-conditions) on Wiley Online Library for rules of use; OA articles are governed by the applicable Creative Commons License

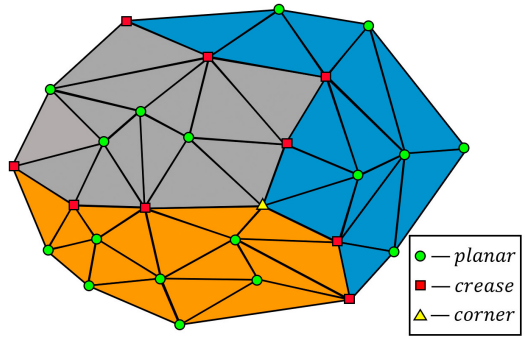

FIGURE 5 Three structural types of the vertex.

$$\mathcal{L}(\mathcal{V}_i) = \begin{cases} \text{planar, if } |\mathcal{S}_i| = 1 \\ \text{crease, if } |\mathcal{S}_i| = 2 \\ \text{corner, if } |\mathcal{S}_i| \geq 3 \end{cases} \tag{11}$$

where $|\mathcal{S}_i|$ is the size of $\mathcal{S}_i$. Once the structural type of vertices was defined, the adjacent primitive pairs can be found by judging whether the two primitives share at least one vertex.

Structural deduction

It is difficult to recover all the missing primitives due to the complexity of structures, and some primitives in the initial mesh are even undetectable by human sight. Hence, we focus here only on the structural deduction for those adjacent primitive pairs that are detected as quasi-parallel. An adjacent primitive pair is detected as quasi-parallel and denoted as $\mathcal{Q}\{\overline{r}_l, \overline{r}_r\}$ if it satisfies:

$$Angle(\overline{\mathcal{P}}_l, \overline{\mathcal{P}}_r) \leq \vartheta \tag{12}$$

where $\overline{\mathcal{P}}_l$ and $\overline{\mathcal{P}}_r$ are the corresponding planar models of $\overline{r}_l$ and $\overline{r}_r$, respectively, ϑ is the threshold of the angle for the definition of quasi-parallel.

The structural deduction is based on the existing planar primitive set. For a detected $\mathcal{Q}\{\overline{r}_l, \overline{r}_r\}$, we collect all the shared vertices and group them according to their continuity. The candidate planar model of a shared vertex group $\mathbb{G} = \{\mathcal{V}_1, \ldots, \mathcal{V}_n\}$ is obtained by the following equation:

$$\overline{\mathcal{P}}_c = \underset{\overline{\mathcal{P}}_j \in \mathbb{P}, Angle(\overline{\mathcal{P}}_j, \overline{\mathcal{P}}_k) > \vartheta, Angle(\overline{\mathcal{P}}_j, \overline{\mathcal{P}}_r) > \vartheta}{\operatorname{argmin}} \frac{\sum_{\mathcal{V}_i \in \mathbb{G}} (dist(\mathcal{V}_i, \overline{\mathcal{P}}_j) - \mu)^2}{N_{\mathbb{G}}} \tag{13}$$

where $\mathbb{P} = \{\overline{\mathcal{P}}_1, \ldots, \overline{\mathcal{P}}_n\}$ is the existing planar model set (including those not extracted as valid primitives), $dist(\mathcal{V}_i, \overline{\mathcal{P}}_j)$ is the Euclidean distance between $\mathcal{V}_i$ and $\overline{\mathcal{P}}_j$, μ is the population mean of $dist(\mathcal{V}_i, \overline{\mathcal{P}}_j)$ and $N_{\mathbb{G}}$ is the size of $\mathbb{G}$. As illustrated in Figure 6, two deduction types are distinguished according to the adjacent relationship between $\mathcal{Q}$ and $\overline{\mathcal{P}}_c$'s corresponding primitive $\overline{r}_c$:

1. $\overline{r}_c$ is selected as the completion primitive if $\overline{r}_c$ is valid and adjacent to $\overline{r}_l$ or $\overline{r}_r$.

14779730, 2023, 181, Downloaded from https://onlinelibrary.wiley.com/doi/10.1111/phor.12438 by Wuhan University, Wiley Online Library on [08/03/2024]. See the Terms and Conditions (https://onlinelibrary.wiley.com/terms-and-conditions) on Wiley Online Library for rules of use; OA articles are governed by the applicable Creative Commons License

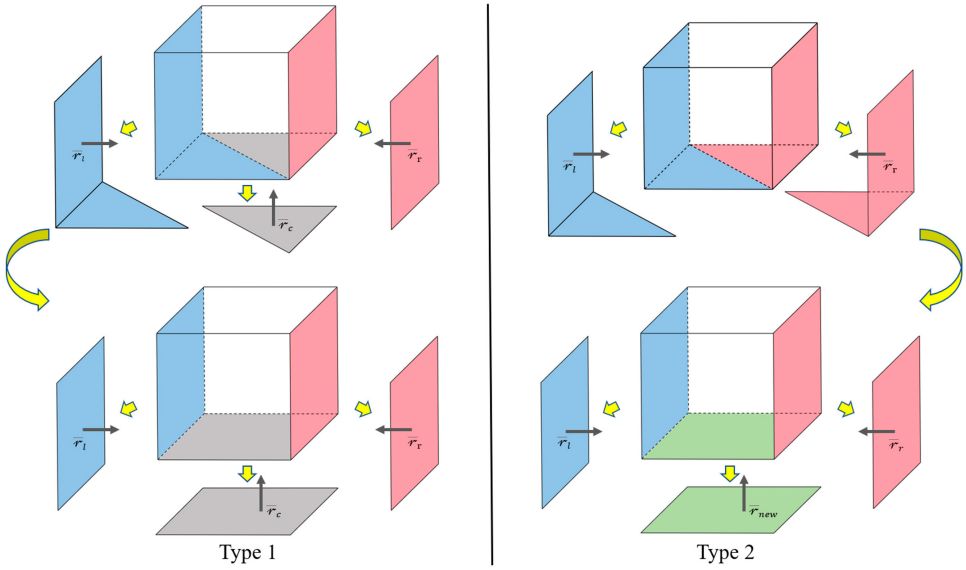

FIGURE 6 Adjacency typology and corresponding deduction results. The deduction is conducted in two different manners according to whether the candidate primitive (coloured in grey) is adjacent to the quasi-parallel adjacent primitive pair (coloured in blue and red). The candidate primitive is used as the deduction result if it is adjacent (left). Otherwise, a new primitive will be calculated (right).

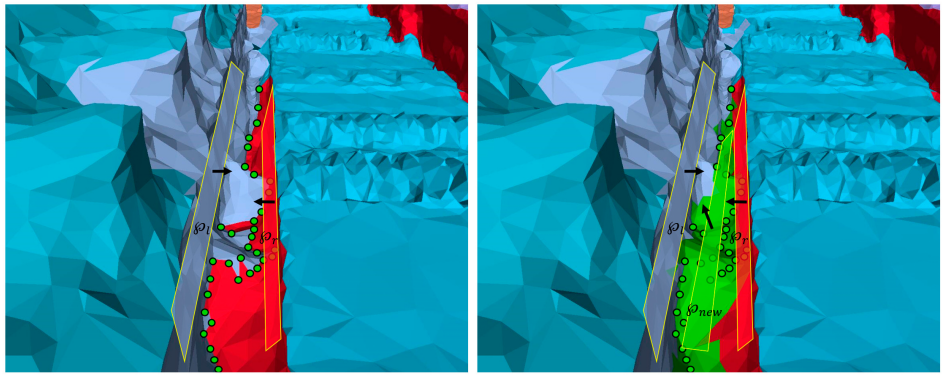

FIGURE 7 Structural deduction case: (a) the primitive determination result and (b) the structural deduction result.

2. A new planar primitive $\overline{\mathcal{F}}_{new}$ is deduced as a completion primitive if $\overline{\mathcal{F}}_c$ is not valid or not adjacent to $\overline{\mathcal{F}}_l$ and $\overline{\mathcal{F}}_r$. The parameters a, b, c of $\overline{\mathcal{P}}_{new}$ (the corresponding planar model of $\overline{\mathcal{F}}_{new}$) are set to the same as $\overline{\mathcal{P}}_c{}'$s, the parameter d of $\overline{\mathcal{P}}_{new}$ is calculated according to the mean coordinate of $\mathbb{G}$.

After the deduction result (i.e., completion primitive) of $\mathcal{Q}\{\overline{\mathcal{F}}_l, \overline{\mathcal{F}}_r\}$ is obtained, we collect the 1-ring neighbour faces of all the vertices in $\mathbb{G}$ and re-partition those faces whose associated primitive is $\overline{\mathcal{F}}_l$ or $\overline{\mathcal{F}}_r$ into the completion primitive. Then gradual region growing is employed for the completion primitive, where adjacent faces that belong to $\overline{\mathcal{F}}_l$ and $\overline{\mathcal{F}}_r$ are assumed to be unlabelled. Figure 7 illustrates an example of this structural deduction.

14779730, 2023, 181, Downloaded from https://onlinelibrary.wiley.com/doi/10.1111/phor.12438 by Wuhan University, Wiley Online Library on [08/03/2024]. See the Terms and Conditions (https://onlinelibrary.wiley.com/terms-and-conditions) on Wiley Online Library for rules of use; OA articles are governed by the applicable Creative Commons License

An adjacent primitive pair (represented in purple and red) is detected as quasi-parallel and contains a group of shared vertices (represented as green circles), as shown in Figure 7a. A new planar primitive (represented in green) and its corresponding new planar model are obtained by structural deduction, and the faces satisfying the aforementioned conditions are re-partitioned into the completion primitive, as shown in Figure 7b.

Iterative completion

The global structure cannot be completed by a single structural deduction process because some of the detected quasi-parallels may miss more than one primitive, which will lead to new quasi-parallels in the deduction results. To address this problem, we designed an iterative process to complete all the missing primitives for those quasi-parallels.

There are three steps in each iteration. Firstly, all the quasi-parallels are detected from the adjacent primitive pair set. Then, the completion primitive (type 1 or type 2 as shown in Figure 6) for each quasi-parallel is deduced using the aforementioned structural deduction. Finally, the adjacency relationships between the primitives are further optimised by the following procedure:

1. For each planar primitive, we collect its inlier vertices and project them onto the corresponding planar models in turn. The first iteration only projects the *planar* vertices, and the subsequent iterations project the *planar*, *crease* and *corner* vertices.
2. The faces that satisfy $Angle(\mathcal{F}_i, \overline{\mathcal{P}}_i) > \theta_{min}$, where $\overline{\mathcal{P}}_i$ is the associated planar model of $\mathcal{F}_i$, are reset to the unlabelled state and then relabelled using a gradual region growing process.

For illustration, Figure 8 shows the results of the first iteration and the final iteration representing the accomplishment of structural completion. Due to the occlusion of non-planar structures, the adjacency relationships of the segmented primitives around the occlusion area may be incorrect. The first iteration, which only projects the *planar* vertices, can solve this problem effectively, as shown in Figure 8a. For this model, all the quasi-parallels are completed after two iterations. Three new planar primitives are obtained from the quasi-parallel shown in the enlarged region of Figure 8b through structural deduction.

Polygonal mesh reconstruction

Since we have obtained building primitives with complete structure and clear adjacency through the previous steps, this section is to assemble the primitives to reconstruct a polygonal mesh. Similar to those

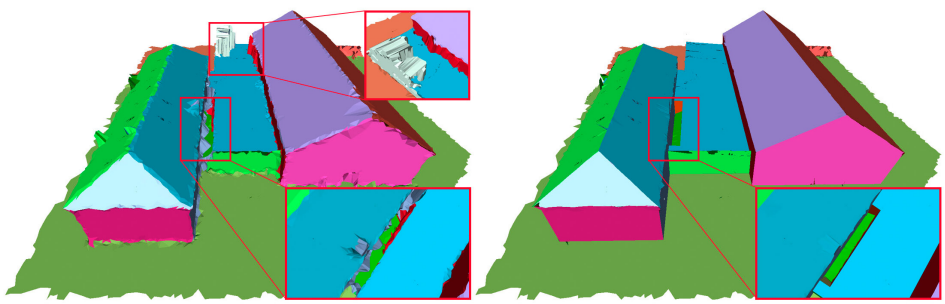

FIGURE 8 Iterative completion case: (a) the first iteration results and (b) the final structural completion results.

14779730, 2023, 181, Downloaded from https://onlinelibrary.wiley.com/doi/10.1111/phor.12438 by Wuhan University, Wiley Online Library on [08/03/2024]. See the Terms and Conditions (https://onlinelibrary.wiley.com/terms-and-conditions) on Wiley Online Library for rules of use; OA articles are governed by the applicable Creative Commons License

connectivity methods that analyse an adjacency graph between planar shapes (Bauchet & Lafarge, 2020), our method assembles the primitives through the adjacency graph composed of corner vertices and primitives.

Specifically, all the corner vertices are selected as the candidate nodes of the polygonal mesh. To ensure the integrity and approximate the original structure, the border vertices in the outer contour of the original input mesh are collected and added to the set of nodes. For each primitive, the corner nodes are linked according to their associated planar primitives while the border nodes are linked according to their original adjacency. The final linkage results of a primitive follow these two principles:

1. One node is only linked with the other two nodes.
2. All the linked polygonal edges are free of self-intersections.

In the section "Gradual region growing", primitives can be separated due to the face discontinuities (see Figure 3). The projection operation in structural completion makes it possible for some edges on these separated primitives to coincide. Hence, it should be noted that these separated primitives with coincidental edges will be combined in this part.

In general, the proposed method not only inherits the efficiency of the connectivity method but also can address linkage errors through structural completion, which enables it to have strong robustness to generate concise and complete models from various challenging data. As illustrated in Figure 9, the final polygonal mesh is concise and approximates the input mesh well. Besides, the outer contour is also retained to better represent the original structure.

EXPERIMENTS AND ANALYSIS

The proposed method was implemented in C++ with the VCG library (http://vcg.isti.cnr.it/vcglib/) for mesh operation and CGAL (https://www.cgal.org/) for Efficient RANSAC usage. To evaluate the performance of the proposed method, several experiments were conducted with various mesh datasets. The experiments were conducted on one core of an Intel® Core™ i7-4770 @ 3.40 GHz CPU, with 16 GB RAM.

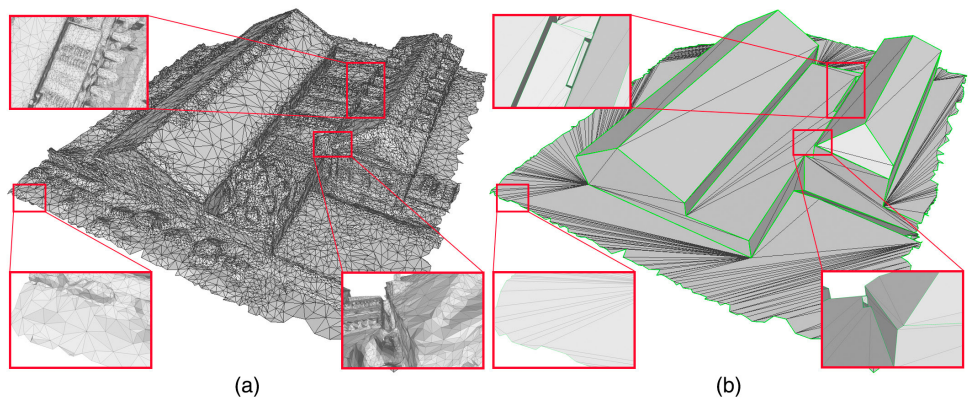

FIGURE 9 Comparison of the input mesh and the final polygonal mesh: (a) the input mesh and (b) the final polygonal mesh. The three enlarged areas are examples of structural completion (top left), free of self-intersection (bottom left) and linkage principle (bottom right).

14779730, 2023, 181, Downloaded from https://onlinelibrary.wiley.com/doi/10.1111/phor.12438 by Wuhan University, Wiley Online Library on [08/03/2024]. See the Terms and Conditions (https://onlinelibrary.wiley.com/terms-and-conditions) on Wiley Online Library for rules of use; OA articles are governed by the applicable Creative Commons License

Experimental results

We applied our proposed method to a variety of building mesh models with different planar connectivity, noise levels and structural complexities. To better show the performance of the fidelity of the results, we calculated the Hausdorff distances (Guthe et al., 2005) between the original mesh and the simplified result, which are shown in different colours on the original mesh. Figure 10 shows the outcomes of primitive determination, polygonal mesh reconstruction and visualisation of the Hausdorff distance for six selected building mesh models (Triumphal Arch, Block, Dormitory, Cluster, House_a and House_b). Triumphal Arch is commonly used for mesh simplification experiments (Salinas et al., 2015). Block, House_a and House_b, which are much more distorted and have a high level of noise, were provided by the corresponding demo of Bouzas et al. (2020). Dormitory, which is located in Guangzhou University Town, was generated by aerial photogrammetry techniques. Cluster is generated from the Dublin ALS data (Laefer et al., 2015).

Table 1 shows the parameter settings of our method, which was set by trial and error. Parameter λ controlled the number and fineness of the initial planar primitive extraction results. It was set according to the minimum area required for the primitive without adjacency. Parameters μ and θ_{sta} affect the efficiency of

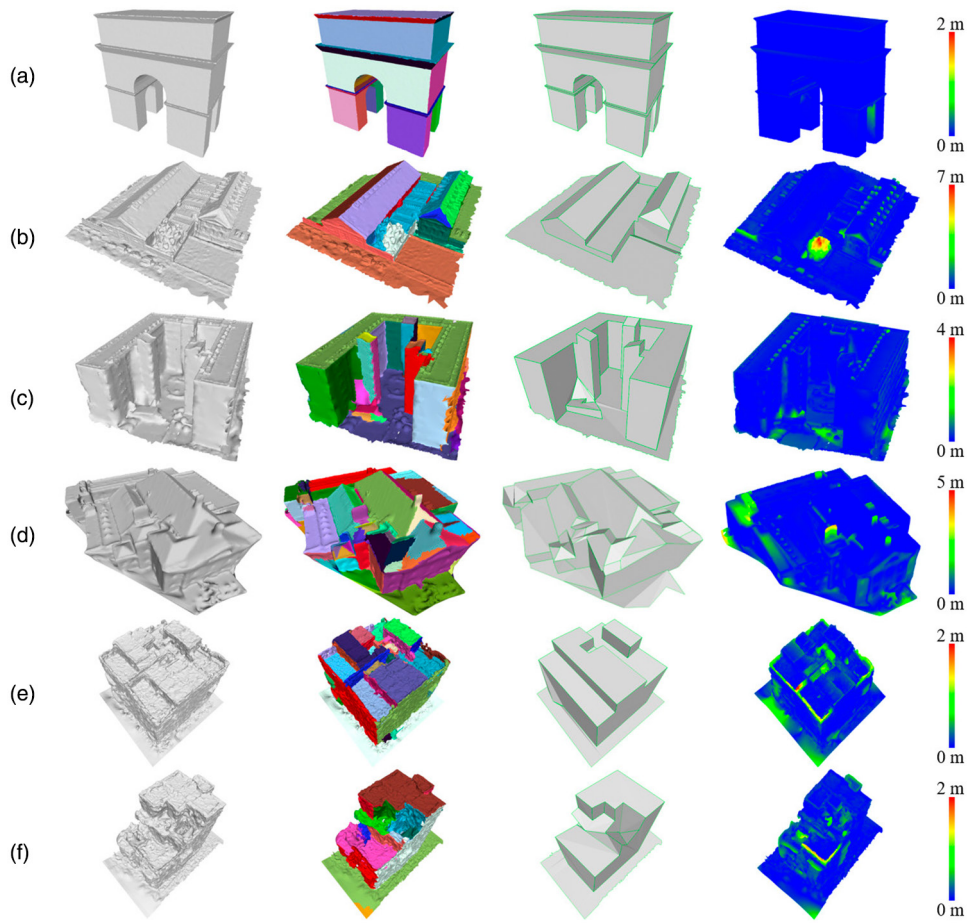

FIGURE 10 Experimental results: (a) Triumphal Arch, (b) Block, (c) Dormitory, (d) Cluster, (e) House_a and (f) House_b. From left to right: Original mesh, primitive determination result, polygonal mesh reconstruction result, and the visualisation of the Hausdorff distance defined between the original mesh and the result.

14679730, 2023, 181, Downloaded from https://onlinelibrary.wiley.com/doi/10.1111/phor.12438 by Wuhan University, Wiley Online Library on [08/03/2024]. See the Terms and Conditions (https://onlinelibrary.wiley.com/terms-and-conditions) on Wiley Online Library for rules of use; OA articles are governed by the applicable Creative Commons License

TABLE 1 The parameters of the proposed method.

Parameter	Descriptor	Value
λ	The threshold of the conditional equation for planar primitive extraction	0.93
μ	The growth coefficient of gradual region growing	1.5
θ_{sta}	The initial angle threshold of gradual region growing	10°
ϑ	The angle threshold of quasi-parallel detection	20°

gradual region growing. Specifically, increasing μ and θ_{sta} can improve the efficiency, but the accuracy may decrease. As the criterion of a quasi-parallel, ϑ affects the preservation of some structure details to a certain extent.

Triumphal Arch is much cleaner than the others, we successfully get its best result, as shown in Figure 10a. Block, Dormitory and Cluster are comprised of multiple buildings and conjoined buildings. The surfaces of these two meshes are unsmooth because they contain various small structures and occlusions. As shown in Figure 10b–d, the proposed method successfully extracted precise planar primitives and generated concise building models while retaining the main structures of the buildings, including the occlusion parts (vegetation etc.). These three data had "quasi-parallel" cases in the primitive determination results due to the existence of some undetectable primitives, and they were completed in the final results. Generally, the proposed method was shown to be capable of generating concise building models that are consistent with the main structure of the original dense meshes and do not have structural defects, even when the original meshes contain unsmooth surfaces, occlusions and some other challenges.

House_a and House_b are two distorted building meshes with high noise levels. Although the overall structures are not complex, the high noise levels they contain make the generation of concise models very challenging. As shown in Figure 10e,f, the proposed method achieved strong robustness in primitive determination and captured many detailed planar structures, even though some of the structures were not reconstructed due to complete failure, the main structures of these buildings were well preserved. These two results demonstrate that our method can adapt to mesh models with high noise levels.

Quantitative evaluation

To evaluate the performance of the proposed method for concise building model generation, we compiled statistics concerning simplicity, fidelity and efficiency (Bauchet & Lafarge, 2020). The simplicity was quantified by the compression ratio between the number of simplified faces to the number of original faces. The fidelity was measured by calculating the mean and the root mean square (RMS) value of the Hausdorff distances. The efficiency of our method was measured by the running times.

The statistics for the evaluation indexes of simplicity and fidelity are listed in Table 2. The number of planar primitives, original faces, simplified faces, original vertices and simplified vertices are denoted as $N_{\bar{\mathcal{F}}}$, $N^o_{\mathcal{F}}$, $N^s_{\mathcal{F}}$, N^o_V and N^s_V, respectively. The compression ratio of face and vertex are denoted as $CR_{\mathcal{F}}$ and CR_V, respectively. The compression ratio of Block was larger than the others (less than 1% for face and 1.5% for vertex) because Block contained a large proportion of border vertices on the outer contour, which were preserved in the simplified results and led to numerous faces. Besides, both the mean and the RMS of the Hausdorff distances of Block were larger than those of other buildings, because vegetation occlusions contained in Block are removed such that the main structure of the building is restored, which leads to larger Hausdorff distances. Furthermore, various small elements in Block and Dormitory were removed in the simplified results, which also made the Hausdorff distances larger.

14779730, 2023, 181, Downloaded from https://onlinelibrary.wiley.com/doi/10.1111/phor.12438 by Wuhan University, Wiley Online Library on [08/03/2024]. See the Terms and Conditions (https://onlinelibrary.wiley.com/terms-and-conditions) on Wiley Online Library for rules of use; OA articles are governed by the applicable Creative Commons License

TABLE 2 Statistics on the evaluation indexes of simplicity and fidelity.

Data	$N_{\bar{\mathcal{F}}}$	$N^o_{\mathcal{F}}$	$N^s_{\mathcal{F}}$	$CR_{\mathcal{F}}$	N^o_V	N^s_V	CR_V	Hausdorff distance (m)	
								Mean	RMS
Triumphal Arch	59	27,258	205	0.75%	13,631	114	0.84%	0.068	0.272
Block	25	47,030	544	1.15%	23,794	507	2.13%	0.458	1.004
Dormitory	37	108,489	527	0.48%	54,310	487	0.89%	0.345	0.401
Cluster	66	88,037	300	0.34%	44,040	179	0.41%	0.320	0.435
House_a	21	39,948	230	0.57%	20,000	202	1.01%	0.148	0.209
House_b	19	37,269	262	0.70%	18,721	234	1.25%	0.157	0.210

TABLE 3 Statistics on running times.

Data	Running times (s)			
	Primitive determination	Structural completion	Reconstruction	Total
Triumphal Arch	0.792	0.566	0.713	2.071
Block	5.820	2.437	2.037	10.295
Dormitory	16.182	6.420	5.047	27.640
Cluster	7.291	3.549	3.021	13.861
House_a	1.451	1.508	0.754	3.713
House_b	1.499	0.383	0.731	2.614

Table 3 lists the running times for the experimental buildings, including the running time of each step and the total running time. Note that the plane segmentation process for the vertices was not included in the running time. Table 2 shows that the running time for Dormitory was longer than those of others, especially for the primitive determination step. Because Dormitory has more faces, as well as its irregularity greatly increases the iteration times of gradual region growing.

Performance comparison

Since edge collapse is the most commonly used operation in generating simplified meshes, we compared our method's results on the meshes of Block and Dormitory with the results of the three other available edge-collapse-based methods: (1) the GH method (Garland & Heckbert, 1997), (2) the LT method (Lindstrom & Turk, 1999) and (3) the SLA method (Salinas et al., 2015). GH, LT and SLA were implemented using the demo program of Salinas et al. (2015) and were run on the same machine as our method. In this comparison, the compression ratio of the results was set to 1% for the edge-collapse-based methods, and the default settings were used to set the other parameters.

Figure 11 shows the performance comparison between our method and the three other edge-collapse-based methods. Table 4 lists their corresponding quantitative results. From the perspective of building reconstruction, the proposed method not only approximates the main structure of the original mesh in a concise form, but also removes the occluded features of non-building structures and restores the corresponding building structures. For the two meshes where the surfaces were unsmooth due to various small structures and

14779730, 2023, 181, Downloaded from https://onlinelibrary.wiley.com/doi/10.1111/phor.12438 by Wuhan University, Wiley Online Library on [08/03/2024]. See the Terms and Conditions (https://onlinelibrary.wiley.com/terms-and-conditions) on Wiley Online Library for rules of use; OA articles are governed by the applicable Creative Commons License

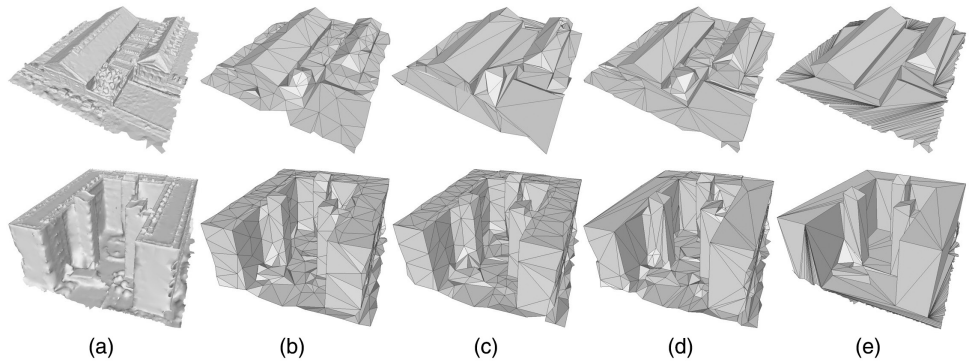

FIGURE 11 Performance comparison on Block (top row) and Dormitory (bottom row): (a) original meshes, (b) results of GH method, (c) results of LT method, (d) results of SLA method and (e) results of our method.

TABLE 4 Performance comparison of the results of Block and Dormitory.

Data	Method	N_F^o	N_F^s	N_V^o	N_V^s	Hausdorff distance (m)		Running time (s)
						Mean	RMS	
Block	GH	47,030	415	23,794	238	0.241	0.442	1.247
	LT		445		238	0.197	0.399	8.059
	SLA		392		238	0.247	0.475	12.643
	Ours		544		507	0.458	1.004	10.295
Dormitory	GH	108,489	1014	54,310	544	0.222	0.303	2.985
	LT		1014		544	0.221	0.302	5.058
	SLA		992		544	0.179	0.298	30.414
	Ours		527		487	0.345	0.401	27.640

occlusions, the performance of our method as far as the Hausdorff distances was not dominant because the Hausdorff distances of the simplified results based on edge collapse were much smaller than ours in some undesired structures. For example, the structures of vegetation and façade windows were still composed of multiple faces in the results of the other methods while our method only retained the main structures. Generally, the other methods could not obtain a structured model and could not always avoid structural defects of the concise mesh. Compared to the other methods, our method was able to obtain a structured model that retained the main structure of the original building and each of the building primitives was reconstructed most simply while preserving the initial adjacency relationships. In terms of efficiency, both our method and the SLA method required more time for primitive extraction, and our method's time was slightly better than that of the SLA method.

Although the edge-collapse-based methods obtained high fidelity simplification results for meshes with low noise levels, effective simplified results cannot be guaranteed when handling highly distorted meshes. To further compare the performance of our method to the other methods, we also conducted concise building model generation using different methods on the meshes of Block, House_a and House_b. PolyFit (Nan & Wonka, 2017) is the most popular plane assembling method and has been proven to be robust. BLN (Bouzas et al., 2020) is a recently proposed building mesh polygonisation method that can generate compact models from multi-view stereo (MVS) building meshes. PolyFit was implemented using its corresponding open-source code, and the results of BLN were

14779730, 2023, 181, Downloaded from https://onlinelibrary.wiley.com/doi/10.1111/phor.12438 by Wuhan University, Wiley Online Library on [08/03/2024]. See the Terms and Conditions (https://onlinelibrary.wiley.com/terms-and-conditions) on Wiley Online Library for rules of use; OA articles are governed by the applicable Creative Commons License

found in the corresponding demo of Bouzas et al. (2020). It is worth noting that PolyFit, BLN and our method are all based on the extracted planar primitives and ultimately generated a structured model. In this comparison, we used the same plane segmentation results for PolyFit and our method.

Figure 12 shows the performance comparison results and Table 5 lists the corresponding quantitative results. PolyFit sliced the primitive bounding box by the planes, which made it rely heavily on the plane segmentation results and produced redundant faces. In this experiment, we adjusted the parameters of plane segmentation to make PolyFit produce satisfactory results. As shown in Figure 12, the polygonal

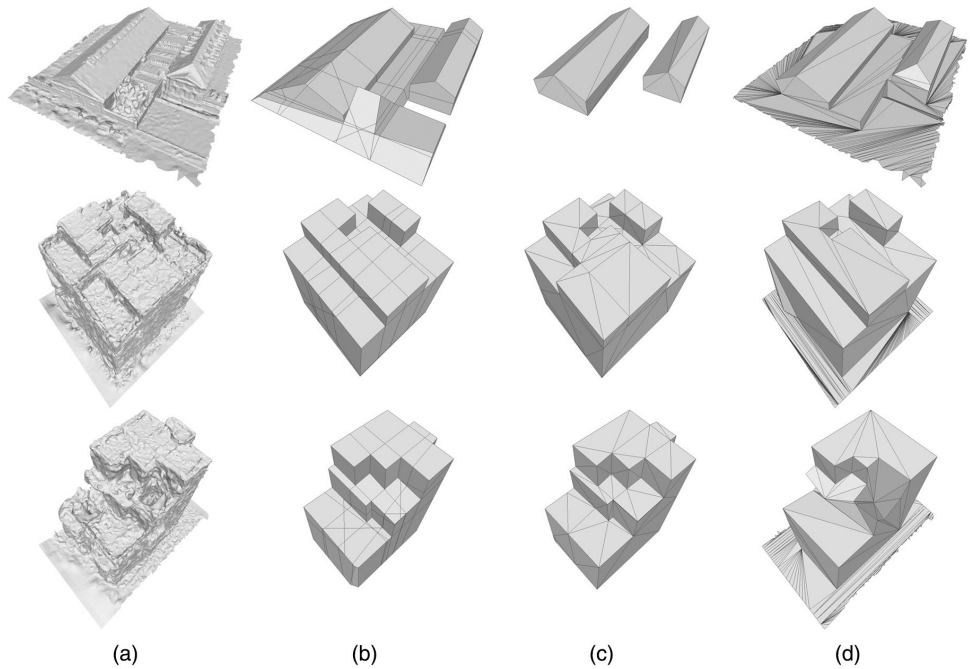

FIGURE 12 Performance comparison on Block (top row), House_a (middle row) and House_b (bottom row): (a) original mesh, (b) results of PolyFit method, (c) results of the BLN method and (d) results of our method.

TABLE 5 Performance comparison of the results of Block, House_a and House_b.

Data	Method	$N_{\mathcal{F}}^{o}$	$N_{\mathcal{F}}^{s}$	N_{V}^{o}	N_{V}^{s}	Hausdorff distance (m)		Running time (s)
						Mean	RMS	
Block	PolyFit	47,030	338	23,794	329	0.725	1.386	489.813
	BLN		32		20	3.806	4.778	/
	Ours		544		507	0.458	1.004	10.295
House_a	PolyFit	39,948	276	20,000	258	0.216	0.339	20.137
	BLN		128		66	0.208	0.325	/
	Ours		230		230	0.148	0.209	3.713
House_b	PolyFit	37,269	344	18,721	226	0.338	0.606	38.455
	BLN		100		52	0.341	0.603	/
	Ours		262		234	0.157	0.210	2.614

14779730, 2023, 181, Downloaded from https://onlinelibrary.wiley.com/doi/10.1111/phor.12438 by Wuhan University, Wiley Online Library on [08/03/2024]. See the Terms and Conditions (https://onlinelibrary.wiley.com/terms-and-conditions) on Wiley Online Library for rules of use; OA articles are governed by the applicable Creative Commons License

meshes produced by our method were structurally more complete and more accurate than those of the other methods. The Hausdorff distances listed in Table 5 substantiate this conclusion. As shown in the top row of Figure 12b,c, both PolyFit and BLN lost some structural details when the original mesh was highly complex. More specifically, there were many structural errors in the results of PolyFit due to the extension of the primitives, such as the left roof of Block and fill the concave part in House_b. The building structure obtained by BLN was incomplete, the low building in the middle of Block and the triangular roof were lost. All three methods showed good robustness for the high noise level meshes (middle row and bottom row of Figure 12). However, structural errors still existed in the results of BLN on House_a (middle row of Figure 12c) due to the hard constraints in BLN's optimisation process. Furthermore, our method was the only one to complete and reconstruct the structural defects, including the connection portion between the two adjacent buildings in Block (top row of Figure 12d) and the recessed portion in House_b (bottom row of Figure 12d). In addition, the computational efficiency of our method was much higher than that of PolyFit, as shown in Table 5.

Sensitivity analysis

The threshold of the conditional equation for planar primitive extraction (λ) is an essential parameter that influenced the local structural accuracy of the final results. Our experiments revealed that the reasonable setting range of λ is from 0.8 to 0.99; and while a large set of λ results in fewer detailed structures, a small set of λ is likely to produce redundant structures.

Different settings of λ were used for the Block mesh in Figure 13. The main structures of the four results were in good agreement with the original mesh. With an increase of λ, the number of planar primitives and the fineness of the local structures decreased.

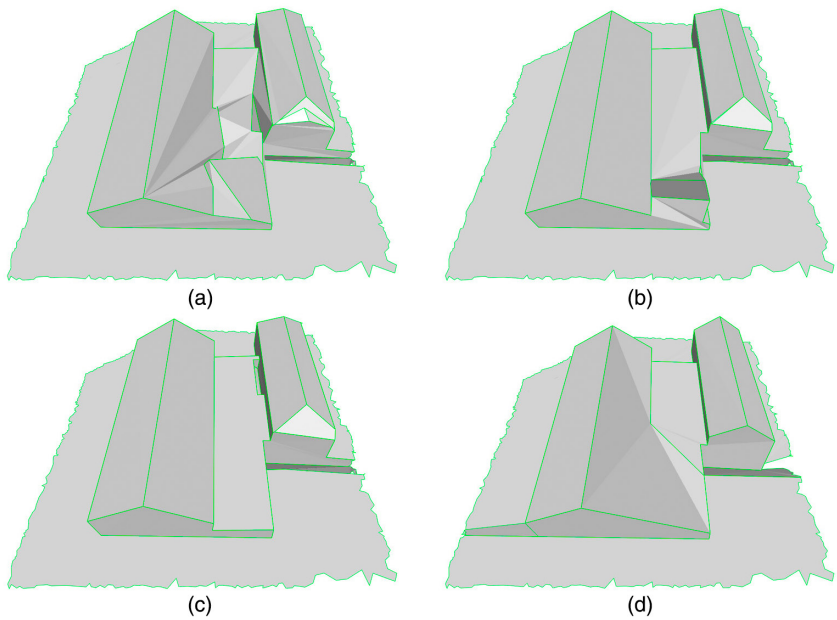

FIGURE 13 Experimental results of our proposed method under different settings of λ: (a) $\lambda = 0.83$, (b) $\lambda = 0.88$, (c) $\lambda = 0.93$ and (d) $\lambda = 0.98$.

14779730, 2023, 181, Downloaded from https://onlinelibrary.wiley.com/doi/10.1111/phor.12438 by Wuhan University, Wiley Online Library on [08/03/2024]. See the Terms and Conditions (https://onlinelibrary.wiley.com/terms-and-conditions) on Wiley Online Library for rules of use; OA articles are governed by the applicable Creative Commons License

Limitations

The proposed primitive determination and structural completion approach effectively improved the approximation and integrity of the reconstructed building model, even when there were some undetectable planar primitives in the original mesh. However, for some complex fine structures, multiple continuous

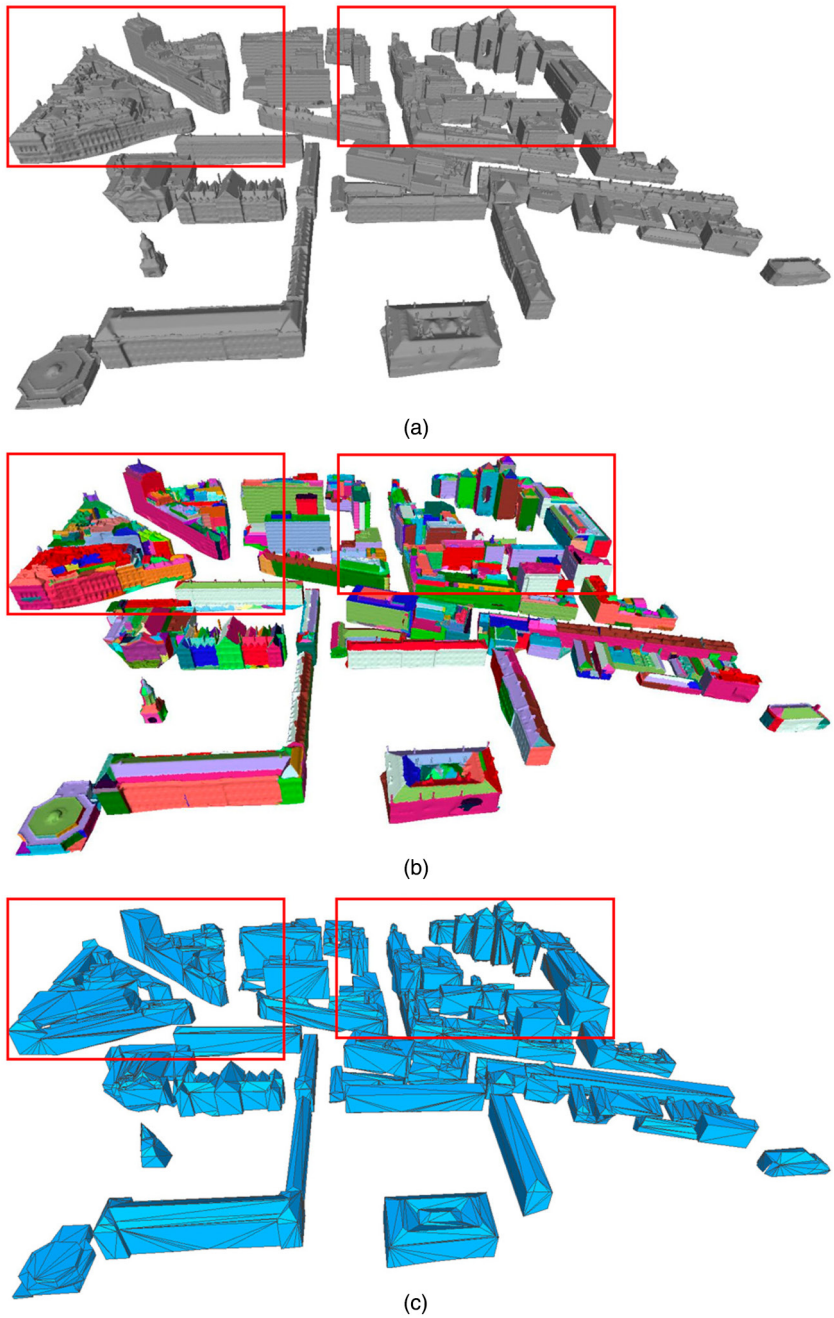

FIGURE 14 Application to urban building modelling: (a) input building models generated from airborne laser scanning point clouds (3,304,990 faces), (b) primitive determination results and (c) concise building models generated by our method (6626 faces).

14779730, 2023, 181, Downloaded from https://onlinelibrary.wiley.com/doi/10.1111/phor.12438 by Wuhan University, Wiley Online Library on [08/03/2024]. See the Terms and Conditions (https://onlinelibrary.wiley.com/terms-and-conditions) on Wiley Online Library for rules of use; OA articles are governed by the applicable Creative Commons License

primitives may not be detected, which can lead to persistent incorrect adjacencies in the primitive determination results. For such cases, it is difficult to complete these missing continuous primitives. Hence, the fineness of the overall structure still relies on the initially detected planes to a certain extent. Moreover, our method can only solve the occlusion problems for some non-building structures that are not too large and have no detected meaningful primitives. If the non-building structure is too large, the corresponding primitives of the occluded building structure may not be detected, which causes incorrect structure in the results. If the non-building structure contains meaningful primitives, redundant non-building structures may be reconstructed in the results. Using the mesh classification as preprocessing to remove the primitives on the non-building structures may be able to improve this problem, but the classification technique is also a difficult task.

APPLICATION TO URBAN BUILDING MODELLING

Figure 14 shows a concrete application of our method in concise urban building modelling. Our method aims to reconstruct concise building models based on high-density building meshes. The original dataset we used was comprised of airborne laser scanning point clouds for Dublin City Centre that were obtained by Laefer et al. (2015). Through building extraction (Lafarge & Mallet, 2012), building instance segmentation (Zhang et al., 2021) and surface reconstruction (Cernea, 2021), the mesh of each building was reconstructed and taken as an input for our proposed method.

Figures 15 and 16 further show the enlarged areas corresponding to the red rectangles in Figure 14. The enlarged figures show that the concise urban building modelling results show good performance by our method in

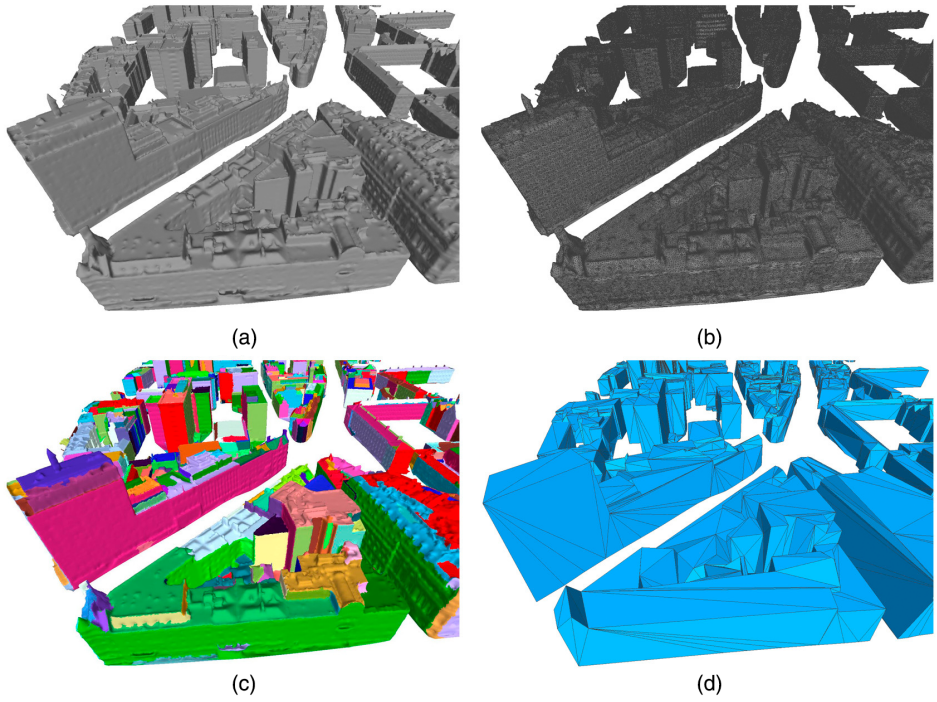

FIGURE 15 The enlarged area corresponding to the left red rectangle in Figure 14: (a) input building models generated from airborne laser scanning point clouds, (b) input building models generated from airborne laser scanning point clouds (with triangles), (c) primitive determination results and (d) concise building models.

14779730, 2023, 181, Downloaded from https://onlinelibrary.wiley.com/doi/10.1111/phor.12438 by Wuhan University, Wiley Online Library on [08/03/2024]. See the Terms and Conditions (https://onlinelibrary.wiley.com/terms-and-conditions) on Wiley Online Library for rules of use; OA articles are governed by the applicable Creative Commons License

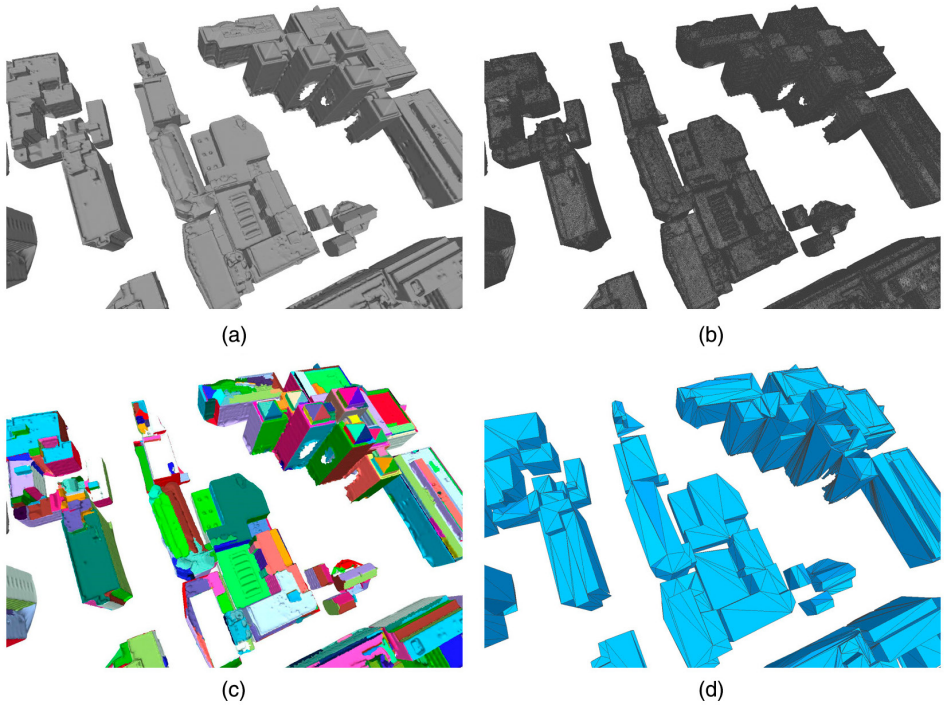

FIGURE 16 The enlarged area corresponding to the right red rectangle in Figure 14: (a) input building models generated from airborne laser scanning point clouds, (b) input building models generated from airborne laser scanning point clouds (with triangles), (c) primitive determination results and (d) concise building models.

both simplicity and fidelity. More specifically, the number of faces was reduced from 3.15 M to only 6.6 k, and the mean value of the Hausdorff distance was 0.36 m.

CONCLUSIONS

This paper presented a novel method for generating concise building models from dense meshes. Considering the diversity of planar structures, an a contrario model was constructed that can accurately extract planar primitives. The proposed primitive determination approach further partitions the remaining faces into the primitives by a two-stage gradual region growing strategy so that the adjacency relationships between the primitives can be obtained. Then, structural completion is used to solve the problem of primitive loss and structural defects. The final concise building model was generated by connectivity-based primitive assembling. Our method preserves and recovers the main structure of the original dense building mesh to the greatest extent possible. When compared to other planar primitive-based methods, our method was shown to be much less dependent on the segmentation of planes.

The experiments we conducted on a variety of building models revealed that our method was effective in generating concise building models whether or not the original dense mesh was closed and whether or not there were structural defects. We also demonstrated the applicability of our method in large-scale city modelling, where most of the buildings are very complicated.

Our future work will focus on classifying original dense meshes, thus eliminating redundant primitives on non-building structures. We also intend to investigate a better way to extract non-planar primitives to reconstruct the non-planar structures of buildings.

14757730, 2023, 181, Downloaded from https://onlinelibrary.wiley.com/doi/10.1111/phor.12438 by Wuhan University, Wiley Online Library on [08/03/2024]. See the Terms and Conditions (https://onlinelibrary.wiley.com/terms-and-conditions) on Wiley Online Library for rules of use; OA articles are governed by the applicable Creative Commons License

ACKNOWLEDGEMENTS

This work was in part supported by the Basic Research Strengthening Program of China (173 Program) with Grant No. 2020-JCJQ-ZD-015-00-04, the National Natural Science Foundation of China with Grant No. 41871368, the Science and Technology Major Project of Hubei Province with Grant No. 2021AAA010 and Zhizhuo Research Fund on Spatial–Temporal Artificial Intelligence (Grant No. ZZJJ202206).

ORCID

Xinyi Liu https://orcid.org/0000-0001-5333-8054
Yongjun Zhang https://orcid.org/0000-0001-9845-4251

REFERENCES

Almansa, A., Desolneux, A. & Vamech, S. (2003) Vanishing point detection without any a priori information. *IEEE Transactions on Pattern Analysis and Machine Intelligence*, 25(4), 502–507. Available from: https://doi.org/10.1109/TPAMI.2003.1190575

Arikan, M., Schwarzler, M., Flory, S., Wimmer, M. & Maierhofer, S. (2013) O-snap: optimization-based snapping for modeling architecture. *ACM Transactions on Graphics*, 32(1), 1–15. Available from: https://doi.org/10.1145/2421636.2421642

Awwad, T.M., Zhu, Q., Du, Z. & Zhang, Y. (2010) An improved segmentation approach for planar surfaces from unstructured 3D point clouds. *Photogrammetric Record*, 25(129), 5–23. Available from: https://doi.org/10.1111/j.1477-9730.2009.00564.x

Bauchet, J.P. & Lafarge, B. (2020) Kinetic shape reconstruction. *ACM Transactions on Graphics*, 39(5), 1–14. Available from: https://doi.org/10.1145/3376918

Besl, P.J. & Jain, R.C. (1988) Segmentation through variable-order surface fitting. *IEEE Transactions on Pattern Analysis and Machine Intelligence*, 10(2), 167–192. Available from: https://doi.org/10.1109/34.3881

Biljecki, F., Stoter, J., Ledoux, H., Zlatanova, S. & Çöltekin, A. (2015) Applications of 3D city models: state of the art review. *ISPRS International Journal of Geo-Information*, 4(4), 2842–2889. Available from: https://doi.org/10.3390/ijgi4042842

Biosca, J.M. & Lerma, J.L. (2008) Unsupervised robust planar segmentation of terrestrial laser scanner point clouds based on fuzzy clustering methods. *ISPRS Journal of Photogrammetry and Remote Sensing*, 63, 84–98. Available from: https://doi.org/10.1016/j.isprsjprs.2007.07.010

Boulch, A., Gorce, M.D.L. & Marlet, R. (2014) Piecewise-planar 3D reconstruction with edge and corner regularization. *Computer Graphics Forum*, 33(5), 55–64. Available from: https://doi.org/10.1111/cgf.12431

Bouzas, V., Ledoux, H. & Nan, L. (2020) Structure-aware building mesh polygonization. *ISPRS Journal of Photogrammetry and Remote Sensing*, 167, 432–442. Available from: https://doi.org/10.1016/j.isprsjprs.2020.07.010

Bruno, F., Bruno, S., De Sensi, G., Luchi, M.-L., Mancuso, S. & Muzzupappa, M. (2010) From 3D reconstruction to virtual reality: a complete methodology for digital archaeological exhibition. *Journal of Cultural Heritage*, 11(1), 42–49. Available from: https://doi.org/10.1016/j.culher.2009.02.006

Bughin, E. & Almansa, A. (2010) Planar patch detection for disparity maps. In: *Proc. 3DPVT*. Espace Saint Martin: IEEE Computer Society.

Cernea, D. (2021) *OpenMVS: open multi-view stereo reconstruction library*. Available from: https://github.com/cdcseacave/openMVS [Accessed 13th September 2021].

Chauve, A.L., Labatut, P. & Pons, J.P. (2010) Robust piecewise-planar 3D reconstruction and completion from large-scale unstructured point data. *2010 IEEE Computer Society Conference on Computer Vision and Pattern Recognition*, 1, 1261–1268. Available from: https://doi.org/10.1109/CVPR.2010.5539824

Chen, J. & Chen, B. (2008) Architectural modelling from sparsely scanned range data. *International Journal of Computer Vision*, 78(2–3), 223–236. Available from: https://doi.org/10.1007/s11263-007-0105-5

Cohen, J., Manocha, D. & Olano, M. (2003) Successive mappings: an approach to polygonal mesh simplification with guaranteed error bounds. *International Journal of Computational Geometry and Applications*, 13(1), 61–94. Available from: https://doi.org/10.1142/S0218195903001074

Cohen-Steiner, D., Alliez, P. & Desbrun, M. (2004) Variational shape approximation. *ACM Transactions on Graphics*, 23(3), 905–914. Available from: https://doi.org/10.1145/1015706.1015817

Desolneux, A., Moisan, L. & Morel, J.-M. (2007) *From gestalt theory to image analysis: a probabilistic approach*. New York: Springer Science & Business Media.

Dong, Z., Yang, B., Hu, P. & Scherer, S. (2018) An efficient global energy optimization approach for robust 3D plane segmentation of point clouds. *ISPRS Journal of Photogrammetry and Remote Sensing*, 137, 112–133. Available from: https://doi.org/10.1016/j.isprsjprs.2018.01.013

Garland, M. & Heckbert, P.S. (1997) Surface simplification using quadric error metrics. *Proceedings of the 24th Annual Conference on Computer Graphics and Interactive Techniques, SIGGRAPH '97*, 44, 209–216.

14779730, 2023, 181, Downloaded from https://onlinelibrary.wiley.com/doi/10.1111/phor.12438 by Wuhan University, Wiley Online Library on [08/03/2024]. See the Terms and Conditions (https://onlinelibrary.wiley.com/terms-and-conditions) on Wiley Online Library for rules of use; OA articles are governed by the applicable Creative Commons License

Guthe, M., Borodin, P. & Klein, R. (2005) Fast and accurate Hausdorff distance calculation between meshes. *Journal of WSCG*, 13(2), 41–48.

Laefer, D.F., Abuwarda, S., Vo, A.V., Linh, T.H. & Gharibi, H. (2015) *Aerial laser and photogrammetry survey of Dublin city collection record*. Available from: https://geo.nyu.edu/catalog/nyu-2451-38684

Lafarge, F. & Alliez, P. (2013) Surface reconstruction through point set structuring. *Computer Graphics Forum*, 32(2), 225–234. Available from: https://doi.org/10.1111/cgf.12042

Lafarge, F. & Mallet, C. (2012) Creating large-scale city models from 3D point clouds: a robust approach with hybrid representation. *International Journal of Computer Vision*, 99(1), 69–85. Available from: https://doi.org/10.1007/s11263-012-0517-8

Li, M. & Nan, L. (2021) Feature-preserving 3D mesh simplification for urban buildings. *ISPRS Journal of Photogrammetry and Remote Sensing*, 173, 135–150. Available from: https://doi.org/10.1016/j.isprsjprs.2021.01.006

Li, Y., Wu, X., Chrysathou, Y., Sharf, A., Cohen-Or, D. & Mitra, N.J. (2020) GlobFit: consistently fitting primitives by discovering global relations. *ACM Transactions on Graphics*, 30(4), 1–12. Available from: https://doi.org/10.1145/1964921.1964947

Lindstrom, P. (2000) Out-of-core simplification of large polygonal models. *Proceedings of the 27th Annual Conference on Computer Graphics and Interactive Techniques*, *SIGGRAPH* '00, 31, 259–262.

Lindstrom, P. & Turk, G. (1999) Evaluation of memoryless simplification. *IEEE Transactions on Visualization and Computer Graphics*, 5(2), 98–115. Available from: https://doi.org/10.1109/2945.773803

Marinov, M. & Kobbelt, L. (2005) Automatic generation of structure preserving multiresolution models. *Computer Graphics Forum*, 24(3), 479–486. Available from: https://doi.org/10.1111/j.1467-8659.2005.00873.x

Monszpart, A., Mellado, N., Brostow, G.J. & Mitra, N.J. (2015) RAPter: rebuilding man-made scenes with regular arrangements of planes. *ACM Transactions on Graphics*, 34(4), 1–12. Available from: https://doi.org/10.1145/2766995

Nan, L. & Wonka, P. (2017) PolyFit: polygonal surface reconstruction from point clouds. In: *2017 IEEE International Conference on Computer Vision (ICCV)*. Washington, DC: IEEE Computer Society, pp. 2372–2380. Available from: https://doi.org/10.1109/ICCV.2017.258

Nguyen, H., Belton, D. & Helmholz, P. (2019) Planar surface detection for sparse and heterogeneous mobile laser scanning point clouds. *ISPRS Journal of Photogrammetry and Remote Sensing*, 151, 141–161. Available from: https://doi.org/10.1016/j.isprsjprs.2019.03.006

Nurunnabi, A., Belton, D. & West, G. (2012) Robust segmentation in laser scanning 3D point cloud data. In: *International Conference on Digital Image Computing Techniques and Applications (DICTA), IEEE*. Washington, DC: IEEE Computer Society, pp. 1–8.

Oesau, S., Lafarge, F. & Alliez, P. (2016) Planar shape detection and regularization in tandem. *Computer Graphics Forum*, 35(1), 203–215. Available from: https://doi.org/10.1111/cgf.12720

Pham, T.T., Chin, T.J., Yu, J. & Suter, D. (2014) The random cluster model for robust geometric fitting. *IEEE Transactions on Pattern Analysis and Machine Intelligence*, 36(8), 1658–1671. Available from: https://doi.org/10.1109/TPAMI.2013.2296310

Rabbani, T., Van Den Heuvel, F. & Vosselmann, G. (2006) Segmentation of point clouds using smoothness constraint. *The International Archives of the Photogrammetry, Remote Sensing and Spatial Information Sciences*, 36(5), 248–253.

Salinas, D., Lafarge, F. & Alliez, P. (2015) Structure-aware mesh decimation. *Computer Graphics Forum*, 34(6), 211–227. Available from: https://doi.org/10.1111/cgf.12531

Sampath, A. & Shan, J. (2006) Clustering based planar roof extraction from LiDAR data. In: *Proceedings of the American Society for Photogrammetry and Remote Sensing Annual Conference, Reno, NV, USA*. Reno: American Society for Photogrammetry and Remote Sensing (ASPRS), pp. 5–6.

Schindler, F., Worstner, W. & Frahm, J.M. (2011) Classification and reconstruction of surfaces from point clouds of man-made objects. In: *Proceedings of International Conference on Computer Vision (ICCV) Workshops*. Washington, DC: IEEE Computer Society.

Schnabel, R., Wahl, R. & Klein, R. (2007) Efficient RANSAC for point cloud shape detection. *Computer Graphics Forum*, 26(2), 214–226. Available from: https://doi.org/10.1111/j.1467-8659.2007.01016.x

Sevgen, S.C. & Karsli, F. (2020) An improved RANSAC algorithm for extracting roof planes from airborne LiDAR data. *Photogrammetric Record*, 35(169), 40–57. Available from: https://doi.org/10.1111/phor.12296

Song, J., Xia, S., Wang, J. & Chen, D. (2021) Curved buildings reconstruction from airborne LiDAR data by matching and deforming geometric primitives. *IEEE Transactions on Geoscience and Remote Sensing*, 59(2), 1660–1674. Available from: https://doi.org/10.1109/TGRS.2020.2995732

Tarsha-Kurdi, F., Landes, T. & Grussenmeyer, P. (2007) Hough-transform and extended RANSAC algorithms for automatic detection of 3D building roof planes from LiDAR data. *ISPRS Workshop on Laser Scanning 2007 and SilviLaser 2007, Espoo, Finland*, 36, 407–412.

Vo, A.V., Linh, T.H., Laefer, D.F. & Bertolotto, M. (2015) Octree-based region growing for point cloud segmentation. *ISPRS Journal of Photogrammetry and Remote Sensing*, 104, 88–100. Available from: https://doi.org/10.1016/j.isprsjprs.2015.01.011

14779730, 2023, 181, Downloaded from https://onlinelibrary.wiley.com/doi/10.1111/phor.12438 by Wuhan University, Wiley Online Library on [08/03/2024]. See the Terms and Conditions (https://onlinelibrary.wiley.com/terms-and-conditions) on Wiley Online Library for rules of use; OA articles are governed by the applicable Creative Commons License

von Gioi, R.G., Jakubowicz, J., Morel, J.-M. & Randall, G. (2010) LSD: a fast line segment detector with a false detection control. *IEEE Transactions on Pattern Analysis and Machine Intelligence*, 32(4), 722–732. Available from: https://doi.org/10.1109/TPAMI.2008.300

Wan, Y., Zhang, Y. & Liu, X. (2019) An a-contrario method of mismatch detection for two-view pushbroom satellite images. *ISPRS Journal of Photogrammetry and Remote Sensing*, 153, 123–136. Available from: https://doi.org/10.1016/j.isprsjprs.2019.04.020

Wang, S., Cai, G., Cheng, M., Marcato, J.M., Huang, S., Wang, Z., Su, S.-Z., Li, J. (2020) Robust 3D reconstruction of building surfaces from point clouds based on structural and closed constraints. *ISPRS Journal of Photogrammetry and Remote Sensing*, 170, 29–44. Available from: https://doi.org/10.1016/j.isprsjprs.2020.09.004

Yan, J., Shan, J. & Jiang, W. (2014) A global optimization approach to roof segmentation from airborne LiDAR point clouds. *ISPRS Journal of Photogrammetry and Remote Sensing*, 94, 183–193. Available from: https://doi.org/10.1016/j.isprsjprs.2014.04.022

Yang, B. & Lee, J. (2017) Improving accuracy of automated 3-D building models for smart cities. *International Journal of Digital Earth*, 12(2), 209–227. Available from: https://doi.org/10.1080/17538947.2017.1395089

Zelinka, S. & Garland, M. (2002) Permission grids: practical, error-bounded simplification. *ACM Transactions on Graphics*, 21(2), 207–229. Available from: https://doi.org/10.1145/508357.508363

Zhang, Y., Yang, W., Liu, X., Wan, Y., Zhu, X. & Tan, Y. (2021) Unsupervised building instance segmentation of airborne LiDAR point clouds for parallel reconstruction analysis. *Remote Sensing*, 13(6), 1136. Available from: https://doi.org/10.3390/rs13061136

Zhu, X., Liu, X., Zhang, Y., Wan, Y. & Duan, Y. (2021) Robust 3D plane segmentation from airborne point clouds based on quasi-a-contrario theory. *IEEE Journal of Selected Topics in Applied Earth Observations and Remote Sensing*, 14, 7133–7147. Available from: https://doi.org/10.1109/JSTARS.2021.3093576

How to cite this article: Liu, X., Zhu, X., Zhang, Y., Wang, S. & Jia, C. (2023) Generation of concise 3D building model from dense meshes by extracting and completing planar primitives. *The Photogrammetric Record*, 38, 22–46. Available from: https://doi.org/10.1111/phor.12438

14779730, 2023, 181, Downloaded from https://onlinelibrary.wiley.com/doi/10.1111/phor.12438 by Wuhan University, Wiley Online Library on [08/03/2024]. See the Terms and Conditions (https://onlinelibrary.wiley.com/terms-and-conditions) on Wiley Online Library for rules of use; OA articles are governed by the applicable Creative Commons License